Translational Science

Direct Observation of von Willebrand Factor Elongation and Fiber Formation on Collagen During Acute Whole Blood Exposure to Pathological Flow

Thomas V. Colace, Scott L. Diamond

Objective—In severe stenosis, von Willebrand Factor (vWF) experiences millisecond exposures to pathological wall shear rates (γ_w). We sought to evaluate the deposition of vWF onto collagen surfaces under flow in these environments.

Methods and Results—Distinct from viscometry experiments that last many seconds, we deployed microfluidic devices for single-pass perfusion of whole blood or platelet-free plasma over fibrillar type 1 collagen (<50 ms transit time) at pathological γ_w or spatial wall shear rate gradients (grad γ_w). Using fluorescent anti-vWF, long thick vWF fibers (>20 µm) bound to collagen were visualized at constant γ_w>30 000 s^{-1} during perfusion of platelet-free plasma, a process enhanced by EDTA. Rapid acceleration or deceleration of EDTA platelet-free plasma at grad γ_w=±1.1×10^5 to ±4.3×10^7 s^{-1}/cm did not promote vWF deposition. At 19 400 s^{-1}, EDTA blood perfusion resulted in rolling vWF–platelet nets, although blood perfusion (normal Ca^{2+}) generated large vWF/platelet deposits that repeatedly embolized and were blocked by anti-glycoprotein Ib or the $\alpha_{IIb}\beta_3$ inhibitor GR144053 and did not require grad γ_w. Blood perfusion at venous shear rate (200 s^{-1}) produced a stable platelet deposit that was a substrate for massive but unstable vWF–platelet aggregates when flow was increased to 7800 s^{-1}.

Conclusion—Triggered by collagen and enhanced by platelet glycoprotein Ib and $\alpha_{IIb}\beta_3$, vWF fiber formation occurred during acute exposures to pathological γ_w and did not require gradients in wall shear rate. (***Arterioscler Thromb Vasc Biol.*** 2013;33:105-113.)

Key Words: glycoprotein Ib ■ hemodynamics ■ platelet ■ stenosis ■ von Willebrand Factor

Severe arterial stenoses are sites of extreme flow acceleration and deceleration, where pathological wall shear rates (γ_w) can range from 5000 to >100 000 s^{-1} (wall shear stresses of 150 to >3000 dyne/cm^2).[1–5] More than 75% stenosis is required before a significant flow resistance causes symptoms of angina.[6] Severe stenosis or coarctation can result in a flow recirculation zone in the poststenotic region, with a transition to turbulence and vortex shedding during the deceleration phase of diastole.[5,7,8]

Sites of flow disturbance resulting from complex secondary flows, oscillatory slow flow, reversing flows, or extreme pathological shear rates and shear rate gradients are correlated with endothelial dysfunction.[9] These sites are also predisposed to atherosclerosis, plaque rupture, platelet activation, and thrombosis. Peak spatial gradients in γ_w, grad γ_w=+600 000 s^{-1}/cm (grad wall shear stress, grad τ_w=20 000 dyne cm^{-2} cm^{-1}), are predicted for the inlet to a human coronary artery stenosis.[3] At the exit of a human coronary stenosis, maximal grad γ_w approaches −3×10^6 s^{-1}/cm.[3] Similarly, Schirmer and Malek[4] reported grad τ_w=±20 000 dyne cm^{-2} cm^{-1} in human carotid stenosis (grad γ_w=±570 000 s^{-1}/cm).

At sites of arterial injury, von Willebrand factor (vWF) greatly facilitates platelet capture via tethering through glycoprotein Ib (GPIb) binding.[10] After binding collagen type I or type III, vWF can undergo a conformational change that enhances exposure of the A1 domain to promote GPIb interaction with platelets.[11] The binding of vWF A1 domain to platelet GPIb is essential for platelet adhesion at physiological arterial wall shear rates (>1500 s^{-1}). In patients with von Willebrand disease (vWD) type 3, a condition in which almost no detectable vWF is present, a severe bleeding phenotype is observed.[12]

When sheared continuously in a cone-and-plate viscometer, high concentrations of soluble vWF (100 µg/mL) will undergo aggregation into enormous fibrous aggregates of 32×10^6 molecular weight (MW) (2155 s^{-1} for 30 seconds) to 847×10^6 MW (6000 s^{-1} for 120 seconds).[13] Similarly, shearing in a cone-and-plate viscometer at >2200 s^{-1} for ≈3 minutes will result in shear-induced platelet activation, a phenomenon that requires vWF and platelet release of ADP.[14–17] Ultralarge vWF (uLvWF) is particularly potent in mediating shear-induced platelet activation as observed in a cone-and-plate viscometer.[18] Recirculation of a vWF solution in an air-exposed, piezo-driven recirculation results in vWF unfolding and extension at a critical shear rate >5000 s^{-1}, but the time of exposure needed to observe this response is unknown, and the effect of the air–liquid interface is potentially problematic in the study of

proteins.[19] Steppich et al[20] used 10 to 20× physiological levels of vWF (200 µg/mL) exposed to high shear for a few minutes to create vWF fibril aggregates. Similarly, Barg et al[21] detected vWF fiber formation on collagen after 1-minute perfusion of 10× physiological levels (50 µg/mL) of vWF at 35 dyne/cm^2 (≈5000 s^{-1}), which was not observed at physiological levels of 5 µg/mL vWF.

In contrast to a viscometer or closed-loop recirculation systems, blood is never continually experiencing pathological shear stresses in vivo for many seconds or minutes. Rather, the exposures are extremely brief, and the unfolding or fiber-forming behavior of vWF during exposure to pathological flows is not well studied under such conditions. Using a stenosis microfluidic device, Nesbitt et al[22] reported a role for shear rate gradients as a causative mechanism in local platelet accumulation, which was GPIb-dependent; however, the underlying role of vWF structural changes was not explored. Interestingly, platelet display of P-selectin downstream of a human stenosis can increase relative to the upstream position.[23] Also, patients with severe aortic stenosis (wall shear stress of 118 dyne/cm^2 or ≈4000 s^{-1} shear rate) display a depletion of the largest vWF multimers to yield an acquired von Willebrand syndrome.[24] Similarly, left ventricular assist device patients can experience an acquired vWD.[25,26] As a shear-sensitive molecule, vWF undergoes a conformational change in these extreme hemodynamic environments, enhancing exposure of a concealed site, the A2 domain, which is susceptible to cleavage by the metalloprotease, ADAMTS13.[27] At shear rates exceeding 15 000 s^{-1}, rolling aggregates of discoid platelets have been observed in flow chambers on surfaces of vWF and collagen.[28] These aggregates were independent of integrin function and required soluble vWF.[28] In vivo aggregates of discoid platelets have also been generated downstream of an artificial stenosis in the mouse mesenteric arteriole.[22] In addition to GPIb/vWF interactions, these thrombi were dependent on $\alpha_{IIb}\beta_3$ interactions, suggesting a role for integrin activation. These prior studies, however, did not investigate the structure of vWF during the creation of thrombotic entities.

The present study explores platelet-free plasma (PFP) and whole blood exposure to pathological shear rates during millisecond exposures in a microfluidic injury model of surface fibrillar collagen. We observed that vWF, detected via epifluorescence microscopy, forms massive fiber aggregates on collagen type 1 surfaces under pathological wall shear rate conditions in plasma and whole blood. When platelets are present, platelet–vWF deposits with elongated and aggregated vWF can be achieved at pathological shear rates even in the absence of Ca^{2+}. Unstable and rolling aggregates that contain significant amounts of vWF as fibrous aggregates were also observed. We demonstrate that high shear rate environments lead to vWF deposition, as well as massive and unstable platelet aggregation on platelet surfaces in the presence of Ca^{2+}. These results represent the first real-time visualization of massive vWF fiber deposition under pathophysiologically relevant conditions supported by collagen. Platelet interactions with these vWF aggregates range from firmly adhered monolayers to massive thrombi with embolic potential.

Materials and Methods

Blood Collection and Preparation

Blood was drawn via venipuncture from healthy men, who self-reported as free of any disease or bleeding disorders, as well as any oral medication, for at least 10 days. All blood donors provided informed written consent in accordance with the Internal Review Board of the University of Pennsylvania. Blood was anticoagulated with sodium citrate (Sigma, St. Louis, MO) or D-Phe-Pro-Arg chloromethylketone (PPACK, 100 µmol/L; Haematologic Industries, Essex, VT) to inhibit thrombin. PFP was generated by centrifugation of whole blood at 1000g for 10 minutes. Severe vWD plasma was from George King Biomedical (Overland Park, KS) and contained <1% detectable vWF. For fluorescent detection of vWF, all samples were treated with a fluorescein isothiocyanate–conjugated polyclonal anti-vWF antibody (1 µg/mL; AbD Serotec, Kidlington, United Kingdom). Some samples were treated with 5 mmol/L EDTA (Sigma) to chelate calcium or 40 µg/mL of function-blocking anti-GPIb antibody AK2 (Abcam, Cambridge, MA).[29] When platelet deposition was measured in real-time epifluorescent microscopy, 0.125 µg/mL of fluorescently conjugated monoclonal antibody HIP8 (BD Biosciences, San Jose, CA) was added.[30] In some experiments, the $\alpha_{IIb}\beta_3$ antagonist, GR144053 (Tocris Biosciences, Bristol, United Kingdom) was added (final concentration, 2 µmol/L) to block $\alpha_{IIb}\beta_3$ function.

Microfluidic Flow Experiments

Two types of microfluidic devices were used in this study. First, the straight-channel microfluidic device had a 100-µm wide×60-µm high cross section generated in poly(dimethylsiloxane) (Sylgard; Dow Corning, Midland, MI) as previously described (Figure IA in the online-only Data Supplement).[31] The second type of microfluidic device, the stenosis channel, consisted of a 500-µm wide×60-µm high channel that rapidly constricted to a 15-µm wide×1000-µm long channel (Figure IB and IC in the online-only Data Supplement), before expanding again to a 500-µm wide channel. The entrance and exit to the stenosis region tapered and expanded over a 100-µm distance in an identical nonlinear fashion to prevent boundary layer separation. Whole blood or PFP samples were perfused through either device via withdraw using a syringe pump (Harvard Apparatus, Holliston, MA). Surfaces of equine collagen type 1 (Chronopar; Chronolog, Havertown, PA) were presented to the flow by using a previously described surface-patterning technique (Figure II in the online-only Data Supplement).[30,32] Briefly, a microchannel, 250-µm wide by 5-cm long (which runs perpendicular to flow channels), was affixed to a glass substrate and was filled with a 1 mg/mL collagen solution and immediately rinsed with 0.5% BSA (Sigma) in HEPES-buffered saline (20 mmol/L HEPES, 150 mmol/L NaCl, pH 7.4; Sigma). The patterning device was removed, and the microfluidic device for blood or plasma perfusion was placed on top of the collagen strip. The flow channels were blocked with BSA for at least 30 minutes before sample perfusion. Real-time deposition of vWF fibers was visualized using epifluorescence microscopy. In plasma experiments, vWF fibers were deposited and subsequently washed in BSA, stained with the fluorescently labeled anti-vWF, and visualized. In whole blood experiments, vWF fiber formation was visualized in real time by direct addition of the fluorescent antibody to the perfusion sample. Microfluidic chambers were mounted on an Olympus IX81 inverted microscope (Olympus America, Center Valley, PA) equipped with a charge-coupled device camera (Hamamatsu, Bridgewater, NJ).

Wall shear rates were calculated by evaluating the analytic solution to flow in a rectangular channel[31] using a custom MATLAB (Mathworks, Nattick, MA) script. Furthermore, a 3-dimensional model of the stenosis channel was generated in COMSOL (Burlington, MA) to determine the flow field and wall shear rate in the more complicated entrance and exit regions. COMSOL simulations were confirmed to reproduce the analytic results for steady flow in the straight rectangular regions of the stenosis microfluidic device. The spatial gradient of wall shear rate along the centerline is defined as grad $\gamma_w = \partial \gamma_w / \partial x |_{z=\text{centerline}}$, where the centerline wall shear rate is $\gamma_w = \partial v_x(y)/\partial y |_{y=0}$.

Quantification of vWF Fiber Density and Length

Density of vWF fibers on patterned collagen surfaces was assessed by measuring the number of fibers intersecting a line drawn perpendicular to the flow direction (we refer to this as a line scan). Unless noted, vWF density represents the average of 3 line scans drawn at 10%, 50%, and 90% of the height of the image. Fiber length was assessed by measuring the length of all fibers that intersect the line scan drawn at 50% of the image height.

Results

vWF Fibers Deposit on Collagen Type 1 Surfaces Under Plasma Flow: Effect of Spatial Gradients

Fibrillar collagen type 1 (250 μm wide) was patterned across the inlet to the 15μm region of the stenosis channel or across the outlet from the 15μm region of the stenosis channel. A total of 20 μL of PFP was treated with 5 mmol/L EDTA and perfused through the channels at 3 flow rates: 0.5, 2, or 20 μL/min. These plasma flow rates resulted in maximum centerline wall shear rates of 3000, 12 500, and 125 000 s^{-1}, respectively. Based on the velocity at a height of 150 nm above the surface, plasma transit time across the 250μm collagen patch was 231 ms for a channel cross section of 500 μm and 38 ms at a 15μm cross section for a 20μL/min perfusion. After the 20 μL of plasma was perfused, the surface was rinsed with 0.5% BSA in HEPES-buffered saline and treated with fluorescently labeled anti-vWF and rinsed again for visualization.

Computational fluid dynamics revealed a very steep centerline wall shear rate gradient (grad γ_w) into the constricting and out of the expanding regions of the stenosis microfluidic device (Figure 1A–1C). For a 20μL/min perfusion, this gradient (grad γ_w) was calculated to be ±4.3×10^7 s^{-1}/cm. At 2μL/min perfusion, the centerline grad γ_w was ±4.3×10^6 s^{-1}/cm and at 0.5 μL/min, grad γ_w was ±110 000 s^{-1}/cm.

For centerline wall shear rates of 3000 (Figure 2A and 2D) and 12 500 s^{-1} (Figure 2B and 2E), <5 fibers per line scan were observed, and grad γ_w of ±110 000 to ±4.3×10^6 s^{-1}/cm did not enhance fiber formation in the entrance or exit regions of the stenosis (Figure 2G and 2H). At 20 μL/min, the maximum centerline gradient in wall shear rate was ±4.3×10^7 s^{-1}/cm (Figure 2C and 2F). In the shear gradient region, fiber generation was restricted to regions where the local wall shear rate was >≈30 000 s^{-1} (Figures 1A, 2C, and 2F). There was no marked difference (Figure 2G and 2H) between vWF deposition in the inlet region, the outlet region, or the constant width region (distal to a narrowing or distal to an expansion). The elevated shear rate environment produced long vWF fibers (>100 μm). A constant wall shear rate of 125 000 s^{-1} was sufficient to cause vWF elongation and fiber formation on the surface collagen. An extreme wall shear rate gradient of –4.3×10^7 s^{-1}/cm for a rapidly decelerating flow actually quenched vWF deposition (Figure 2F).

vWF Fibers Deposit on Collagen Type 1 Surfaces Under Plasma Flow: Effect of Calcium

Because vWF and its cleaving protease, ADAMTS13, have calcium-sensitive domains,[33,34] we sought to understand the role of Ca^{2+} in the fiber-deposition process. We compared citrated plasma treated with an additional 5 mmol/L EDTA (≈2 nmol/L free Ca^{2+}) to recalcified, citrated PFP treated with PPACK to prevent thrombin generation. In these experiments, collagen patterning was restricted to the region of 15 μm channel width (Figure 3H, inset). We observed that vWF fibers formed under EDTA conditions were continuous strands >300 nm in width and 100 μm in length at the highest shear rate tested (125 000 s^{-1}; Figure 3C, 3H, and 3I). At lower shear rates (31 200 and 62 400 s^{-1}), the deposition of vWF was significantly reduced, as was fiber length (Figure 3A, 3B, 3H, and 3I). In recalcified, citrated PFP with PPACK, we observed a significant increase in the number of deposited vWF fibers between the lowest and highest shears tested
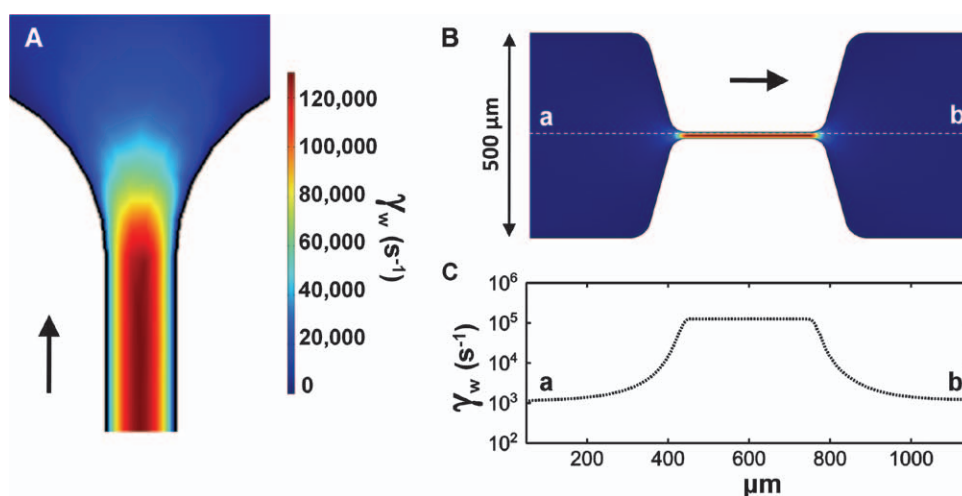

Figure 1. Large wall shear rate gradients are generated in the inlet and outlet of a novel microfluidic model of stenosis. **A,** Computational fluid dynamics defined the wall shear rates in the outlet of the stenosis channel. **B,** A representation of the stenosis channel in COMSOL. The colors indicate local wall shear rate and are equivalent to the scale bar in **A. C,** The local wall shear rate along the centerline of the stenosis channel (dotted white line in B) indicates a steep gradient in centerline wall shear rate (1000–125 000 s^{-1}) at the inlet and outlet of the stenosis (grad γ_w of ±4.3×10^7 s^{-1}/cm).
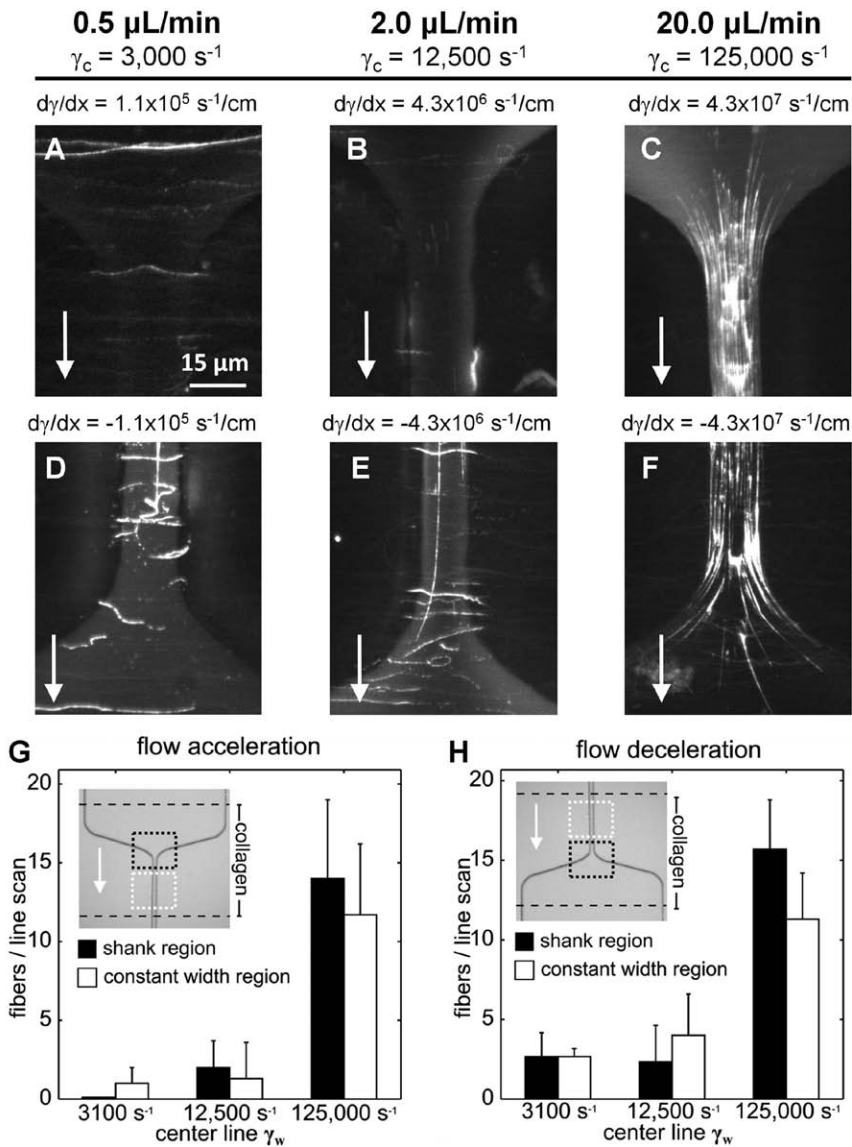
Figure 2. von Willebrand factor (vWF) fibers deposit on surfaces of collagen type 1 in a microfluidic model of coronary stenosis. **A**, Twenty microliter of citrated platelet-free plasma (PFP; plus 5 mmol/L EDTA) was perfused through a microfluidic channel over a collagen type 1 surface at the indicated wall shear rate (**arrow**, flow direction). The collagen surface was localized to the inlet of the stenosis, where a gradient in wall shear rate was present (grad γ_w of 1.1×10^5 s^{-1}/cm). Subsequently, the channel was treated with a fluorescently labeled antibody against vWF and washed. **B** and **C**, The same volume of PFP was perfused through an identical channel at 12 500 and 125 000 s^{-1}, respectively. Few fibers were observed at 12 500 s^{-1}, although many fibers were present at 125 000 s^{-1}. **D** to **F**, The collagen strip was localized to the outlet region of the stenosis, and similar flow conditions were imposed. Few vWF fibers were present at shear rates of ≤12 500 s^{-1}, although many fibers were observed at 125 000 s^{-1}. **G** and **H,** The number of fibers intersecting a line drawn horizontally through the middle of the regions bound by dotted lines (black, shank region; white, constant width region) was counted at each centerline wall shear rate. The results indicate that nonzero grad γ_w in either the inlet or outlet region did not enhance the number of vWF fibers observed compared with the constant width region distal to the shank region. We conclude that acute exposure to an extreme wall shear rate >30 000 s^{-1} is a sufficient criteria for vWF fiber formation on collagen, independent of elongational forces in accelerating or decelerating flows.

(Figure 3D–3F, 3H, and 3I). At the highest shear rate tested (125 000 s^{-1}), the fiber morphology was disjointed compared with EDTA-treated samples, consisting of many strings of different lengths resulting in an average fiber length of 50 μm (Figure 3F and 3I). Citrated PFP (≈40 μm Ca^{2+}) performed identically to PPACK plasma in this experiment (not shown). These results demonstrate that vWF elongated and formed fibers on collagen in a platelet-independent manner, but high wall shear rates (those >30 000 s^{-1}) were required. Removal of calcium enhanced the deposition process. As expected, no deposition of vWF fibers was detected at 125 000 s^{-1} in vWD plasma (Figure III in the online-only Data Supplement).

To confirm that accelerating flows at the stenosis inlet were not strictly necessary for vWF fiber deposition, these experiments were repeated using a constant width device lacking a stenotic region. For both EDTA-treated plasma and EDTA/anti–GPIb-treated whole blood, vWF elongation on collagen was observed (Figures IV and V in the online-only Data Supplement), demonstrating that exposure to an elongational flow was not strictly required for vWF fiber formation on collagen.

vWF Fibers Deposit on Collagen Type 1 Surfaces Under Whole Blood Flow

To avoid spatial wall shear rate gradients in the direction of flow, a larger microchannel with a constant cross section of 100μm wide×60-μm high was used for the study of whole blood flow. Transit times across the 250μm long collagen strip at 150 nm (a near-wall vWF distance) and 3 μm (a near-wall platelet distance) were 61.5 and 3.4 ms, respectively, at a centerline wall shear rate of 19 400 s^{-1}. As was seen with EDTA-PFP, the deposition of long vWF fibers was observed at constant wall shear rate (grad γ_w=0) for perfusion of EDTA whole blood at 19 400 s^{-1} (Figure 4A, EDTA). With EDTA present, large vWF fibers and nets were observed forming on the surface (Figure 4A, PPACK). Even without functional integrins (resulting from chelation of Ca^{2+}), these long fibers had adherent platelets present, although nets seemed to roll on the surface with trapped platelets (Movie I in the online-only Data Supplement). Figure VI in the online-only Data Supplement provides a montage of all of the conditions tested in Figure 4A, with 5 time points per condition.
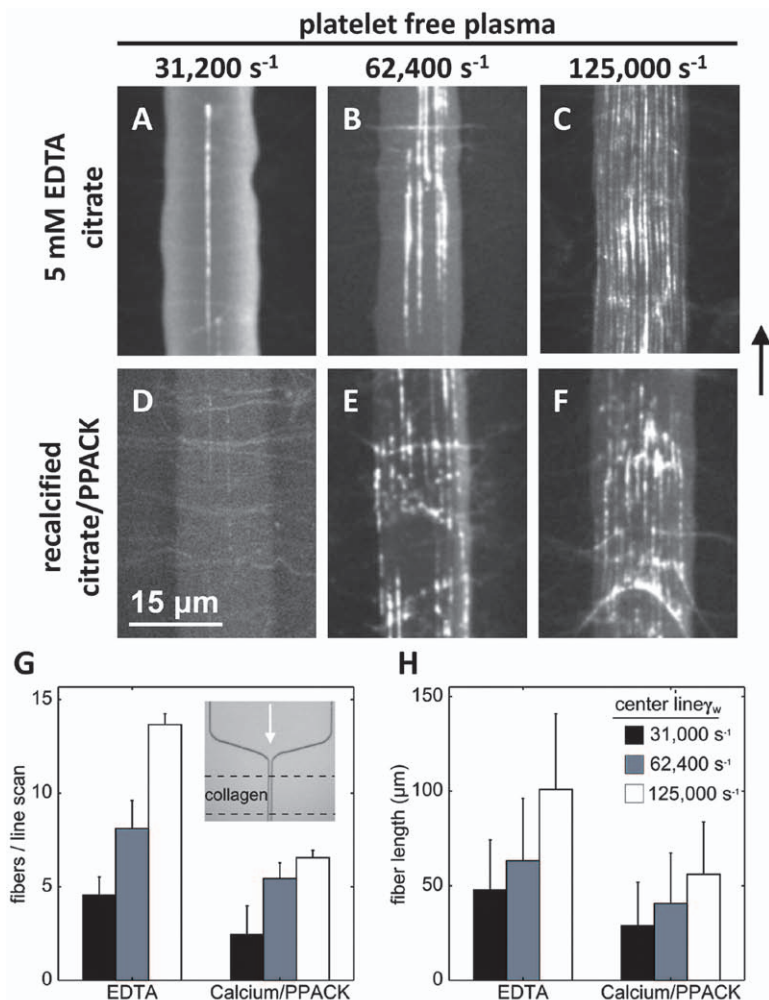
Figure 3. von Willebrand Factor (vWF) fibers deposit on collagen type 1 surfaces in the presence and absence of calcium and were dependent on the wall shear rate. **A** to **C**, Equal quantities of platelet-free plasma (PFP), treated with EDTA (to chelate calcium), were perfused through the stenosis channel at the indicated wall shear rates over a collagen surface restricted to the constant width region. Representative images demonstrate the increase in vWF deposition as the wall shear rate was increased. **D** to **F**, The identical experiment performed in recalcified, citrated PFP treated with D-Phe-Pro-Arg chloromethylketone (PPACK) to prevent thrombin generation. We observed vWF fibers under these conditions as well, which showed a shear-dependent increase in fiber deposition. However, at the highest shear rate tested, the vWF fibers seemed disjointed. **H**, The number of fibers intersecting a horizontal line drawn across the channel (a line scan) was counted and averaged over 3 positions in the channel with 3 replicates per condition. A shear-dependent increase in the number of fibers was observed for all shear rates in the absence of Ca^{2+} ($P<0.02$) and between the lowest and highest shears tested in the presence of Ca^{2+} ($P<0.01$). There was also a significant increase in the number of fibers observed with chelation of Ca^{2+} at the highest and intermediate shear rates ($P<0.03$). **I**, The length of the fibers intersecting a line drawn through the center of the image was averaged for 3 replicates per condition. In EDTA, we observed significant reductions in fiber length between the highest shear rate tested and the intermediate and low shear rate ($P<0.01$). In the presence of Ca^{2+}, a significant increase in fiber length was observed between the lowest and highest shear rates tested ($P<0.01$). Chelation of Ca^{2+} caused a significant increase in fiber length for all shear rates tested ($P<0.03$).

In the presence of Ca^{2+}, functional integrins led to rapid platelet adhesion and embolization (Figure 4A, PPACK). Fibers were observed, although large masses of platelets also stained positive for vWF (Movie II in the online-only Data Supplement). To block $\alpha_{IIb}\beta_3$ platelet–platelet interactions via fibrinogen, a small-molecule inhibitor of $\alpha_{IIb}\beta_3$ was used (2 µmol/L, GR144053; Figure VII in the online-only Data Supplement). This allowed us to replicate the integrin-blocking effects of EDTA without chelating Ca^{2+}. When $\alpha_{IIb}\beta_3$ was inhibited in the presence of Ca^{2+}, large platelet masses were no longer present and faint fibers were seen adhering to the surface at $19\ 400\ s^{-1}$ (Figure 4A, PPACK+GR144053). The vWF fiber formation (normal Ca^{2+}) was more evident when the wall shear rate was increased to $38\ 800\ s^{-1}$ (Figure 4A). The dependency on γ_w of vWF deposition in the presence of PPACK and GR144053 is shown in Figure 4B. At the lowest shear rate tested ($11\ 600\ s^{-1}$), few fibers were observed, although several collagen fibers did stain positively for vWF. Increasing the shear rate to $15\ 500\ s^{-1}$ revealed a modest increase in vWF fibers, although fibers >50 µm required shear rates of $19\ 400\ s^{-1}$. When the wall shear rate was increased to $38\ 800\ s^{-1}$, many vWF fibers were generated on the surface, as well as rolling clumps of vWF and platelets.

Figure 4C presents time course data of vWF fluorescence on the collagen surface under perfusion of whole blood with normal Ca^{2+} (PPACK), PPACK plus GR144053, and PPACK plus 40 µg/mL of a function-blocking antibody against GPIb (AK2). In the absence of inhibitors, large platelet aggregates that were highly vWF-positive (Figure 4C, PPACK) were repeatedly generated and embolized rapidly. With $\alpha_{IIb}\beta_3$ antagonism (2 µmol/L GR144053), larger fibers, as well as nets of vWF and platelets, were detected (Figure 4C, PPACK+GR144053); however, large thrombi were not, resulting in a significant reduction in vWF signal (Figure 4C). In the presence of AK2, formation of vWF fibers was not blocked; however, the large platelet masses and rolling nets of vWF and platelets were completely abolished. This resulted in a significant reduction in vWF signal, as well (Figure 4C, PPACK+ab[AK2] and Figure VIII in the online-only Data Supplement). The presence of platelets in whole blood enhanced the formation of vWF fibers on collagen surfaces under conditions of normal Ca^{2+} (Figure 3B and 3D) for single-pass transit time exposures of 3.4 to 61.5 ms.

vWF Mediates Rapid and Embolic Platelet Adhesion at Pathological Shear Rates

Whole blood anticoagulated with PPACK (normal Ca^{2+}) and treated with fluorescently conjugated anti-vWF and anti-CD41a to label platelets was perfused over a collagen type 1 surface at a venous wall shear of $200\ s^{-1}$. Platelet adhesion had reached a steady state after 1500 seconds of perfusion (Figure 5A[a] and 5C). Very little vWF immunofluorescence and
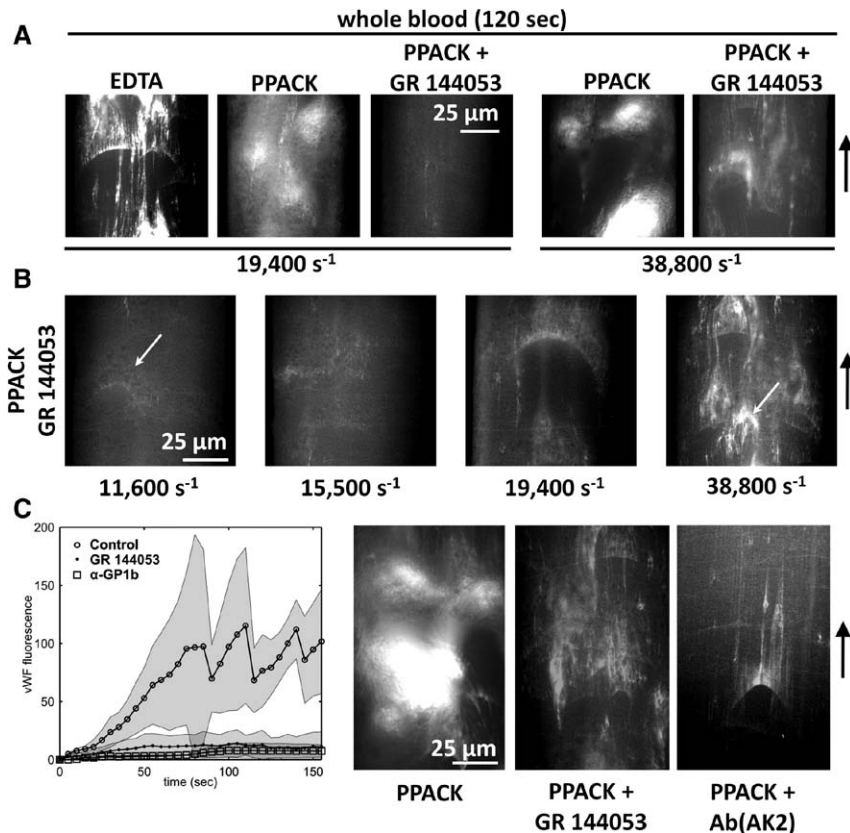
Figure 4. von Willebrand Factor (vWF) fibers deposit on collagen type 1 surfaces during whole blood flow perfusion in a straight-channel geometry. **A**, Whole blood was perfused in the presence of EDTA or normal Ca^{2+} with or without GR144053 to block integrin function at the indicated wall shear rates. At 120 seconds in the absence of Ca^{2+}, long fibers of vWF are detected on the surface, as well as rolling aggregates of vWF and platelets. In the presence of Ca^{2+}, large platelet aggregates form, which embolized rapidly and incorporated vWF. In the absence of integrin function, large aggregates no longer formed, but faint fibers of vWF were seen on the surface, consistent with our previous results indicating that normal Ca^{2+} led to less vWF than EDTA conditions. At 2-fold elevated shear rates, vWF was observed both in platelet aggregates (functioning integrins) and on the surface (blocked integrins). **B**, vWF fiber deposition was a shear-dependent process under normal Ca^{2+} in the absence of integrin function. At the lowest shear tested, firmly adherent platelets were observed (**arrow**), although vWF was not detected. With increasing shear, more vWF was observed on the collagen surface. At the highest shear rate tested, rolling aggregates of vWF and platelets were observed (**arrow**). **C**, vWF fluorescence was measured over a 150-second perfusion of untreated whole blood (D-Phe-Pro-Arg chloromethylketone [PPACK]) at 38 800 s^{-1} or samples treated with GR144053 and a glycoprotein Ib (GPIb) function-blocking antibody (AK2). The results indicate that the large platelet masses formed on the collagen surface enhance vWF capture and require both active $\alpha_{IIb}\beta_3$ integrin and GPIb. The representative images (**right**) demonstrate the vWF fluorescence at the 120-second time point for all conditions. The large platelet masses seen with PPACK vanish with the addition of either inhibitor.

no elongated vWF fibers were observed in the platelet mass formed at venous shear rate (Figure 5B[a] and 5D). At ≈1600 seconds, the flow rate was suddenly increased such that the nominal wall shear rate would have been 7800 s^{-1} in an empty channel, but was several fold higher here because of channel obstruction resulting from the platelet mass.[32] Within 100 seconds of the shear rate increase, massive platelet accumulation had occurred, embolized, and rebounded (Figure 5A[b–d] and 5C). However, upon shear increase, the large platelet masses formed on top of the steady-state surface incorporated vWF (Figure 5B[b and d]). The vWF fluorescence data presented in Figure 5D were normalized to the 1530-second time point. When platelet deposition was reinitiated after the flow increase, a 5-fold increase in vWF was measured. Compared with the 2-fold increase in platelet adhesion, the vWF fluorescence indicated that the high shear rate conditions facilitated the incorporation and accumulation of plasma vWF into the growing but fragile deposit (Figure 5C and 5D).

In a parallel experiment (Figure 6A), a steady-state surface of platelets was generated in an identical manner to that in Figure 5A(a) and was briefly rinsed with HEPES-buffered saline containing 5 mmol/L Ca^{2+} (Figure 6B). PPACK-treated PFP (normal Ca^{2+}) was perfused over the surface at a wall shear rate of 23 400 s^{-1}. Figure 6C demonstrates vWF fibers forming on the surface of the platelet mass. These elongated fibers formed from PFP at pathological shear conditions were

generated on the platelet surface (no collagen present) and are likely the molecular unit responsible for nucleating the massive platelet adhesion events that occur under the pathological shear rate environments, where whole blood was present (Figure 5A[a]) instead of PFP.

Discussion

Long and thick fibers of vWF were visualized as they formed on collagen type 1 surfaces under pathological shear rate conditions. These fibers were present, regardless of the use of fluorescent antibody during the experiment or after perfusion. The observed fibers were collagen-bound. Given their fluorescence width of several pixels (>300 nm), the observed elongated vWF fiber bundles were highly unlikely to be individual extended vWF molecules (30 nm width <1 pixel). Importantly, we observed that these vWF fibers were in a quenched state (ie, bound to collagen), such that they did not relax when flow was stopped. We report that the fiber-deposition process was not sensitive to the elongational flows present at the inlet or the outlet of the stenosis microfluidic device. We conclude that acute exposure to an extreme wall shear rate >30 000 s^{-1} is a sufficient criteria for vWF fiber formation on collagen, independent of elongational forces in accelerating or decelerating flows. High wall shear rate and elongational flows are not mutually exclusive, however, and either or both may be operative in various situations. For
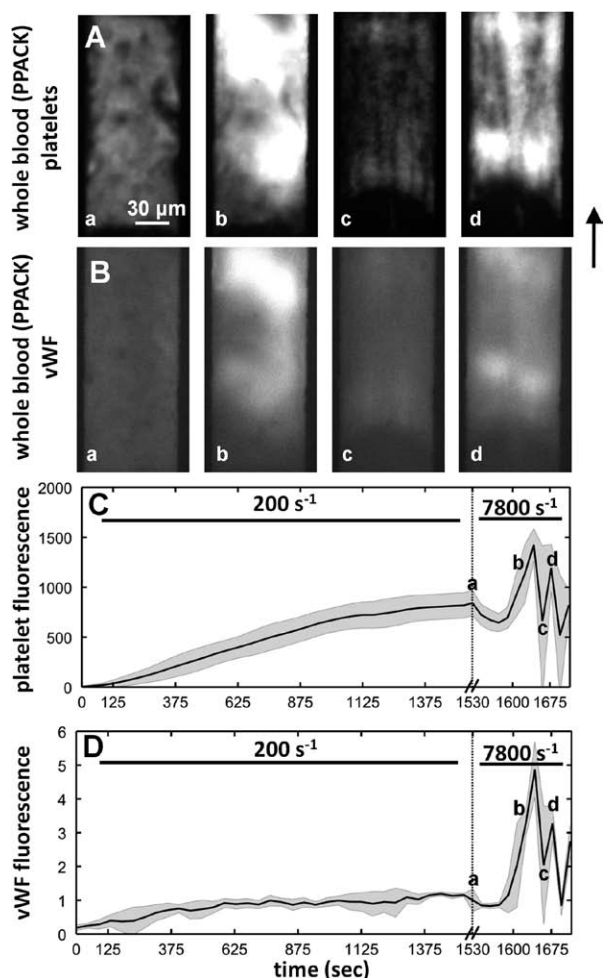
Figure 5. Onset of pathological shear rates triggered formation of massive aggregates that were unstable. **A**, Platelet deposition from whole blood (D-Phe-Pro-Arg chloromethylketone [PPACK]) onto a collagen type 1 surface was monitored over an ≈1530-second time period at an initial venous wall shear rate of 200 s^{-1}. At the 1530 seconds, a stable nongrowing platelet deposit had formed (**a**). The flow rate was suddenly increased such that in an empty channel the local wall shear rate would have been 7800 s^{-1}. Within 100 seconds, massive platelet adhesion had initiated, which resulted in a cycle of thrombus growth and embolization (**b–d**). The images are representative of multiple experiments. **B**, von Willebrand Factor (vWF) content was also measured in the growing platelet aggregates. After 1530 seconds of perfusion, no detectable vWF was present. After the shear rate increase, the massive platelet aggregates that form were highly vWF-positive. **C**, Platelet accumulation was measured by fluorescence at the microfluidic injury site. The gray shading indicates the SD of 4 experiments. Upon shear rate increase (**a**), the fluorescence intensity briefly drops as platelets were torn from the surface, and then recovered in a rapid burst of adhesion. Note the difference in time scales. **D**, vWF accumulation in the growing thrombus as flow was increased. The gray shading indicates the SD of 4 experiments. The fluorescent intensity was normalized to the 1530-second time point. Upon shear rate increase (**a**), vWF was incorporated into the rapidly growing thrombus.

example, in cases of borderline high or pathological arterial wall shear rates (3000–10 000 s^{-1}), elongational flows at sites of stenosis may be relevant to vWF elongation, as well as a driver of enhanced wall-directed platelet fluxes. Furthermore, the process of vWF fiber deposition is distinct from existing literature focused on coil-stretched transitions[35,36] in bulk flow,

as the fiber-generation process described here occurs on the channel wall via collagen (see Discussion in the online-only Data Supplement).

Formation of these fibrils was evident in PPACK-treated whole blood at shear rates of 19 400 s^{-1} but was best visualized at 38 800 s^{-1}. In PFP, the phenomenon had a threshold of ≈30 000 s^{-1}. The absence of Ca^{2+} greatly enhanced the visualization of the fibers. The role of Ca^{2+} may be 2-fold in preventing the aggregation of vWF, as it supports refolding of the vWF A2 domain and is required for ADAMTS13 function.[33,34] We have demonstrated that platelets rapidly accumulate and embolize under conditions of high pathological shear with a mechanism likely related to vWF unfolding and did not require a shear rate gradient. The large and unstable masses incorporate vWF and seem to be nucleated by vWF fibers aggregating on collagen or platelet surfaces. Figure 4C demonstrated that vWF fiber formation and deposition during high-shear whole blood flow was dependent on GPIb and α$_{IIb}$β$_3$. However, platelet aggregation also requires these receptors, and it is difficult to delineate collagen–vWF receptor mechanisms from platelet aggregation–vWF mechanisms under these flow conditions. Because significant vWF fluorescence is associated with the platelet aggregates beyond that formed on the collagen surface, multiple flow-dependent processes may coexist (platelet aggregation, wall-directed platelet fluxes, etc) beyond the direct effect of flow on vWF fiber formation on collagen. The experiment shown in Figure 6 was designed to understand whether high shear rate can cause vWF fiber extension, as platelet mass accumulates. Indeed, elongated fibers were detected at high wall shear rate (Figure 6C), when plasma was perfused over a preexisting platelet deposit. However, this result does not address whether platelet receptors on flowing platelets potentiate vWF elongation and fiber bundle formation. Interestingly, the vWF:platelet ratio increased by a factor of ≈3.3-fold for deposits formed at inlet wall shear rate of 7800 s^{-1} compared with those formed at 200 s^{-1} (Figure 5C and 5D), suggestive of a direct enhancing effect of platelets on vWF deposition at pathological shear rates.

Pathological wall shear rates exceeding 30 000 s^{-1} are predicted in severe stenoses, as well as in left ventricular assist devices.[1–5] Patients with severe aortic stenosis or a left ventricular assist device often present with a bleeding tendency that is linked to loss of the largest vWF multimers. On valve replacement or heart transplant, the distribution of vWF multimers is corrected.[25,37] Recently, Yong et al[23] have demonstrated that platelets respond to the acute exposure of elevated shear, as well. By sampling blood proximal and distal to a variety of coronary stenoses, the authors reported a significant increase in P-selectin exposure downstream of the occlusion, a result that correlated with stenosis severity. In contrast to soluble and globular plasma vWF in physiological hemodynamic conditions, elongated and aggregated vWF fibers formed under the flow conditions in this study may be particularly well suited for multivalent engagement of platelet GPIb, a receptor whose clustering by closely situated A1 domains in the vWF fiber may help drive GPIb-mediated signaling. Generation of vWF fibers may participate in this P-selectin display.
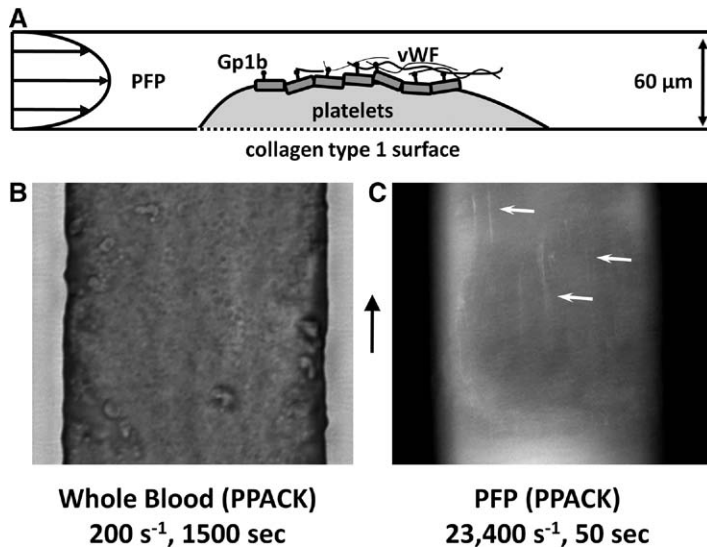
Figure 6. von Willebrand Factor (vWF) fibers deposit on platelet surfaces at pathological shear rates. **A**, A schematic representation of the experimental setup. First, a steady-state platelet surface was deposited on a collagen type 1 surface under whole blood (D-Phe-Pro-Arg chloromethylketone [PPACK]) flow for 1500 seconds at 200 s^{-1}. The flow was then switched to platelet-free plasma (PFP) that was perfused at 23 400 s^{-1}. **B**, A bright field image of the steady-state platelet surface before the perfusion was switched to plasma. **C**, Plasma (PPACK, 1 µg/mL anti-vWF) was perfused over the surface in **B** at 23 400 s^{-1}. After 50 seconds of plasma perfusion, vWF fibers were detected on the platelet surface (**arrows**).

In a recent study, Nesbitt et al[22] suggested that shear gradients drove the formation of a loosely packed discoid platelet aggregate in a microfluidic model of stenosis lacking an adhesive protein surface. The authors demonstrated that no aggregates formed in a channel of constant cross section under the same hemodynamic conditions. They reported that GPIb was required for initial platelet adhesion at the stenosis apex, whereas GPIb and $\alpha_{IIb}\beta_3$ were required for thrombus propagation. In the present study, we have found that rapid formation of loosely packed aggregates did form in channels of constant cross section but required a surface of vWF fiber-coated collagen or platelets. In agreement with the authors, we demonstrate that GPIb can support platelet firm adhesion on these surfaces in the absence of active integrin, but that both are necessary for thrombus propagation. We suggest that the magnitude of γ_w can serve as the driving force behind loosely packed platelet aggregates, a process that requires the elongation and aggregation of vWF bundles on a suitable surface. We have demonstrated that shear rate gradients of ±1.1×10^5 to 4.3×10^7 s^{-1}/cm do not substantially enhance the process of vWF deposition using a microfluidic stenosis model, when perfusing EDTA–PFP over collagen.

Last, we present a role for platelet-bound vWF in thrombogenesis at pathological shear rates. Using a microfluidic channel of constant 100-µm cross section, we generated steady-state thrombi whose ability to capture platelets was restored by a sudden increase in shear rate. We suggest that platelet recruitment was reestablished by enhanced GPIb/vWF tethering resulting from increased vWF self-aggregation at high shear on the thrombus surface. Before the sudden increase in shear rate (Figure 5), the thrombus had grown to create hemodynamic conditions that prevented further platelet attachment and was insufficient to cause vWF fiber formation. After the flow rate increase, vWF fibers formed and were able to support platelet tethering and subsequent activation required for stable adhesion. A similar process was proposed by Kulkarni et al,[38] who illustrated the importance of soluble vWF in platelet adhesion to an immobilized platelet monolayer in the absence of an activating surface, even at venous

shear rates. They suggest that without soluble agonists tethering platelets have less active $\alpha_{IIb}\beta_3$ and require more GPIb/vWF interactions to achieve stable adhesion. Our results are consistent with these earlier findings, and we have visualized the fundamental event of vWF fiber formation that may underlie these prior observations.

During arterial thrombosis at physiological wall shear rates (eg, in mild stenosis with plaque rupture), vWF elongation and fiber formation may initially be minimal. However, as the thrombus growth begins to occlude the vessel and before a significant pressure drop is created by the nonocclusive thrombus (<75% stenosis), the wall shear rates will increase dramatically with a consequent transition to elongated and fibrous vWF-mediating platelet capture. At high pathological shear rates, these nets of vWF and platelets may be less stable and subject to embolism, consistent with a condition of unstable angina or cyclic thrombosis. This study defines precise experimental conditions in which to detect and measure the dynamics of vWF unfolding, vWF fiber elongation, and aggregate formation at pathological shear rates on collagen.

Disclosures
None.

References
1. Li MX, Beech-Brandt JJ, John LR, Hoskins PR, Easson WJ. Numerical analysis of pulsatile blood flow and vessel wall mechanics in different degrees of stenoses. *J Biomech*. 2007;40:3715–3724.
2. Bark DL Jr, Ku DN. Wall shear over high degree stenoses pertinent to atherothrombosis. *J Biomech*. 2010;43:2970–2977.

3. Banerjee RK, Back LH, Back MR, Cho YI. Physiological flow analysis in significant human coronary artery stenoses. *Biorheology*. 2003;40:451–476.

4. Schirmer CM, Malek AM. Patient based computational fluid dynamic characterization of carotid bifurcation stenosis before and after endovascular revascularization. *J Neurointerv Surg*. 2012;4:448–454.

5. Stroud JS, Berger SA, Saloner D. Numerical analysis of flow through a severely stenotic carotid artery bifurcation. *J Biomech Eng*. 2002;124:9–20.

6. Kim HJ, Vignon-Clementel IE, Coogan JS, Figueroa CA, Jansen KE, Taylor CA. Patient-specific modeling of blood flow and pressure in human coronary arteries. *Ann Biomed Eng*. 2010;38:3195–3209.

7. Long Q, Xu XY, Ramnarine KV, Hoskins P. Numerical investigation of physiologically realistic pulsatile flow through arterial stenosis. *J Biomech*. 2001;34:1229–1242.

8. Ojha M, Cobbold RS, Johnston KW, Hummel RL. Detailed visualization of pulsatile flow fields produced by modelled arterial stenoses. *J Biomed Eng*. 1990;12:463–469.

9. Malek AM, Alper SL, Izumo S. Hemodynamic shear stress and its role in atherosclerosis. *JAMA*. 1999;282:2035–2042.

10. Savage B, Saldívar E, Ruggeri ZM. Initiation of platelet adhesion by arrest onto fibrinogen or translocation on von Willebrand factor. *Cell*. 1996;84:289–297.

11. Goto S, Salomon DR, Ikeda Y, Ruggeri ZM. Characterization of the unique mechanism mediating the shear-dependent binding of soluble von Willebrand factor to platelets. *J Biol Chem*. 1995;270:23352–23361.

12. Sadler JE, Budde U, Eikenboom JC, Favaloro EJ, Hill FG, Holmberg L, Ingerslev J, Lee CA, Lillicrap D, Mannucci PM, Mazurier C, Meyer D, Nichols WL, Nishino M, Peake IR, Rodeghiero F, Schneppenheim R, Ruggeri ZM, Srivastava A, Montgomery RR, Federici AB; Working Party on von Willebrand Disease Classification. Update on the pathophysiology and classification of von Willebrand disease: a report of the Subcommittee on von Willebrand Factor. *J Thromb Haemost*. 2006;4:2103–2114.

13. Shankaran H, Alexandridis P, Neelamegham S. Aspects of hydrodynamic shear regulating shear-induced platelet activation and self-association of von Willebrand factor in suspension. *Blood*. 2003;101:2637–2645.

14. Dayananda KM, Singh I, Mondal N, Neelamegham S. von Willebrand factor self-association on platelet GpIbalpha under hydrodynamic shear: effect on shear-induced platelet activation. *Blood*. 2010;116:3990–3998.

15. Peterson DM, Stathopoulos NA, Giorgio TD, Hellums JD, Moake JL. Shear-induced platelet aggregation requires von Willebrand factor and platelet membrane glycoproteins Ib and IIb-IIIa. *Blood*. 1987;69:625–628.

16. Moake JL, Turner NA, Stathopoulos NA, Nolasco L, Hellums JD. Shear-induced platelet aggregation can be mediated by vWF released from platelets, as well as by exogenous large or unusually large vWF multimers, requires adenosine diphosphate, and is resistant to aspirin. *Blood*. 1988;71:1366–1374.

17. Li F, Li CQ, Moake JL, López JA, McIntire LV. Shear stress-induced binding of large and unusually large von Willebrand factor to human platelet glycoprotein Ibalpha. *Ann Biomed Eng*. 2004;32:961–969.

18. Kumar RA, Moake JL, Nolasco L, Bergeron AL, Sun C, Dong JF, McIntire LV. Enhanced platelet adhesion and aggregation by endothelial cell-derived unusually large multimers of von Willebrand factor. *Biorheology*. 2006;43:681–691.

19. Schneider SW, Nuschele S, Wixforth A, Gorzelanny C, Alexander-Katz A, Netz RR, Schneider MF. Shear-induced unfolding triggers adhesion of von Willebrand factor fibers. *Proc Natl Acad Sci USA*. 2007;104:7899–7903.

20. Steppich DM, Angerer JI, Sritharan K, Schneider SW, Thalhammer S, Wixforth A, Alexander-Katz A, Schneider MF. Relaxation of ultralarge VWF bundles in a microfluidic-AFM hybrid reactor. *Biochem Biophys Res Commun*. 2008;369:507–512.

21. Barg A, Ossig R, Goerge T, Schneider MF, Schillers H, Oberleithner H, Schneider SW. Soluble plasma-derived von Willebrand factor assembles to a haemostatically active filamentous network. *Thromb Haemost*. 2007;97:514–526.

22. Nesbitt WS, Westein E, Tovar-Lopez FJ, Tolouei E, Mitchell A, Fu J, Carberry J, Fouras A, Jackson SP. A shear gradient-dependent platelet aggregation mechanism drives thrombus formation. *Nat Med*. 2009;15:665–673.

23. Yong AS, Pennings GJ, Chang M, Hamzah A, Chung T, Qi M, Brieger D, Behnia M, Krilis SA, Ng MK, Lowe HC, Kritharides L. Intracoronary shear-related up-regulation of platelet P-selectin and platelet-monocyte aggregation despite the use of aspirin and clopidogrel. *Blood*. 2011;117:11–20.

24. Vincentelli A, Susen S, Le Tourneau T, Six I, Fabre O, Juthier F, Bauters A, Decoene C, Goudemand J, Prat A, Jude B. Acquired von Willebrand syndrome in aortic stenosis. *N Engl J Med*. 2003;349:343–349.

25. Uriel N, Pak SW, Jorde UP, Jude B, Susen S, Vincentelli A, Ennezat PV, Cappleman S, Naka Y, Mancini D. Acquired von Willebrand syndrome after continuous-flow mechanical device support contributes to a high prevalence of bleeding during long-term support and at the time of transplantation. *J Am Coll Cardiol*. 2010;56:1207–1213.

26. Geisen U, Heilmann C, Beyersdorf F, Benk C, Berchtold-Herz M, Schlensak C, Budde U, Zieger B. Non-surgical bleeding in patients with ventricular assist devices could be explained by acquired von Willebrand disease. *Eur J Cardiothorac Surg*. 2008;33:679–684.

27. Zhang X, Halvorsen K, Zhang CZ, Wong WP, Springer TA. Mechanoenzymatic cleavage of the ultralarge vascular protein von Willebrand factor. *Science*. 2009;324:1330–1334.

28. Ruggeri ZM, Orje JN, Habermann R, Federici AB, Reininger AJ. Activation-independent platelet adhesion and aggregation under elevated shear stress. *Blood*. 2006;108:1903–1910.

29. Dong JF, Berndt MC, Schade A, McIntire LV, Andrews RK, López JA. Ristocetin-dependent, but not botrocetin-dependent, binding of von Willebrand factor to the platelet glycoprotein Ib-IX-V complex correlates with shear-dependent interactions. *Blood*. 2001;97:162–168.

30. Flamm MH, Colace TV, Chatterjee MS, Jing H, Zhou S, Jaeger D, Brass LF, Sinno T, Diamond SL. Multiscale prediction of patient-specific platelet function under flow. *Blood*. 2012;120:190–198.

31. Neeves KB, Maloney SF, Fong KP, Schmaier AA, Kahn ML, Brass LF, Diamond SL. Microfluidic focal thrombosis model for measuring murine platelet deposition and stability: PAR4 signaling enhances shear-resistance of platelet aggregates. *J Thromb Haemost*. 2008;6:2193–2201.

32. Colace TV, Muthard RW, Diamond SL. Thrombus growth and embolism on tissue factor-bearing collagen surfaces under flow: role of thrombin with and without fibrin. *Arterioscler Thromb Vasc Biol*. 2012;32:1466–1476.

33. Anderson PJ, Kokame K, Sadler JE. Zinc and calcium ions cooperatively modulate ADAMTS13 activity. *J Biol Chem*. 2006;281:850–857.

34. Xu AJ, Springer TA. Calcium stabilizes the von Willebrand factor A2 domain by promoting refolding. *Proc Natl Acad Sci USA*. 2012;109:3742–3747.

35. Sing CE, Alexander-Katz A. Globule-stretch transitions of collapsed polymers in elongational flow fields. *Macromolecules*. 2010;43:3532–3541.

36. Sing CE, Alexander-Katz A. Elongational flow induces the unfolding of von Willebrand factor at physiological flow rates. *Biophys J*. 2010;98:L35–L37.

37. Pareti FI, Lattuada A, Bressi C, Zanobini M, Sala A, Steffan A, Ruggeri ZM. Proteolysis of von Willebrand factor and shear stress-induced platelet aggregation in patients with aortic valve stenosis. *Circulation*. 2000;102:1290–1295.

38. Kulkarni S, Dopheide SM, Yap CL, Ravanat C, Freund M, Mangin P, Heel KA, Street A, Harper IS, Lanza F, Jackson SP. A revised model of platelet aggregation. *J Clin Invest*. 2000;105:783–791.